

Ultrafast Lifetime and Bright Emission from Graphene Quantum Dots Using Plasmonic Nanogap Cavities

Hiroyuki Kishida and Maiken H. Mikkelsen*



Cite This: *Nano Lett.* 2022, 22, 904–910



Read Online

ACCESS |



Metrics & More



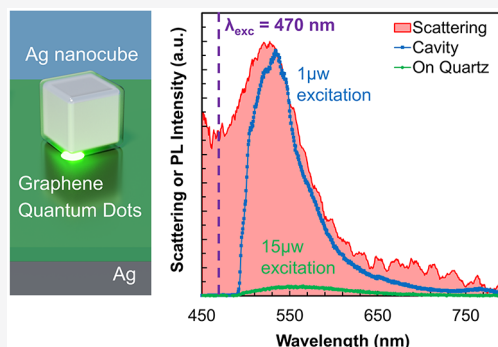
Article Recommendations



Supporting Information

ABSTRACT: Graphene quantum dots (GQDs) are quasi-zero-dimensional, carbon-based luminescent nanomaterials that possess desirable physical properties, such as high photostability, low cytotoxicity, good biocompatibility, and excellent water solubility; however, their long radiative lifetimes significantly limit their use in, e.g., light emitting devices where a fast spontaneous emission rate is essential. Despite a few reports on GQD fluorescence enhancements using metal nanostructures, studies of enhanced spontaneous emission rate remain outstanding. Here, we report fast and bright luminescence by coupling gap plasmon modes to nanoparticle emitters. Through precise control over the nanoparticle's local density of states (LDOS), we achieved a 220-fold increase in the PL intensity. The shortest radiative lifetime obtained was below 8.0 ps and limited by the instrument response, which is over 288-fold shorter than the lifetime of uncoupled GQDs. These findings may benefit the future development of rapid displays and open the possibility of constructing high-frequency classical or quantum telecommunication systems.

KEYWORDS: metal nanostructure, plasmon resonance, metasurface, graphene quantum dots, Purcell factor, nanogap cavities, nanopatch antenna



To date, a wide variety of applications have been reported for graphene quantum dots (GQDs), including heavy-metal-free, high-color-purity deep-blue LEDs,¹ UV photo-detectors,^{2,3} solar cells,⁴ photodynamic therapy,⁵ Hg²⁺ detectors,⁶ single photon emitters,⁷ humidity and pressure sensors,⁸ as well as frequency upconversion.⁹ Despite this broad utility, the typical 2–5 ns radiative lifetimes of GQDs have limited GQD applications in rapid displays and light emitting devices, which demand fast spontaneous emission.¹⁰ In many organic dyes, synthetic structural modifications can shorten radiative lifetimes by inducing either internal (i.e., internal rotation, electron transfer, proton transfer) or external (i.e., Förster and Dexter energy transfer) quenching.¹¹ The rigid structure of GQDs, however, makes many of these well-known techniques difficult to realize in GQD systems. In this work, we instead achieve ultrafast emission by coupling the GQD luminescence to plasmonic gap modes in nanopatch antennas.

Here we demonstrate large emission rate enhancement by coupling GQDs to gap-mode plasmonic cavities, called nanopatch antennas or plasmonic nanogap cavities. Metallic nanostructures with subwavelength features enable unprecedented control of interactions between optical waves and nanoscale materials through the exploitation of localized surface plasmon resonances. Localized surface plasmons confine the incident optical energy into deeply subwavelength

volumes, producing large electric and magnetic field enhancements.

According to Fermi's golden rule, the spontaneous emission rate (γ_{sp}) of an emitter is proportional to the local density of optical states (LDOS)¹²

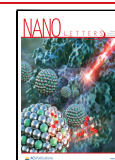
$$\gamma_{sp} = \frac{\pi\omega}{3\hbar\epsilon_0} |p|^2 \rho(r, \omega) \quad (1)$$

where ω is the emission frequency, p is the transition dipole moment of the emitter, r is the position, ϵ_0 is the permittivity of free space, and $\rho(r, \omega)$ is the electromagnetic LDOS at frequency ω . The LDOS can be modified by changing the electromagnetic environment, e.g., by introducing a high- Q cavity or small-mode-volume plasmonic structure. In turn, this modifies the spontaneous emission rate. The enhancement of the spontaneous emission rate of an embedded emitter is quantified by the Purcell factor as follows¹³

Received: September 2, 2021

Revised: December 6, 2021

Published: January 19, 2022



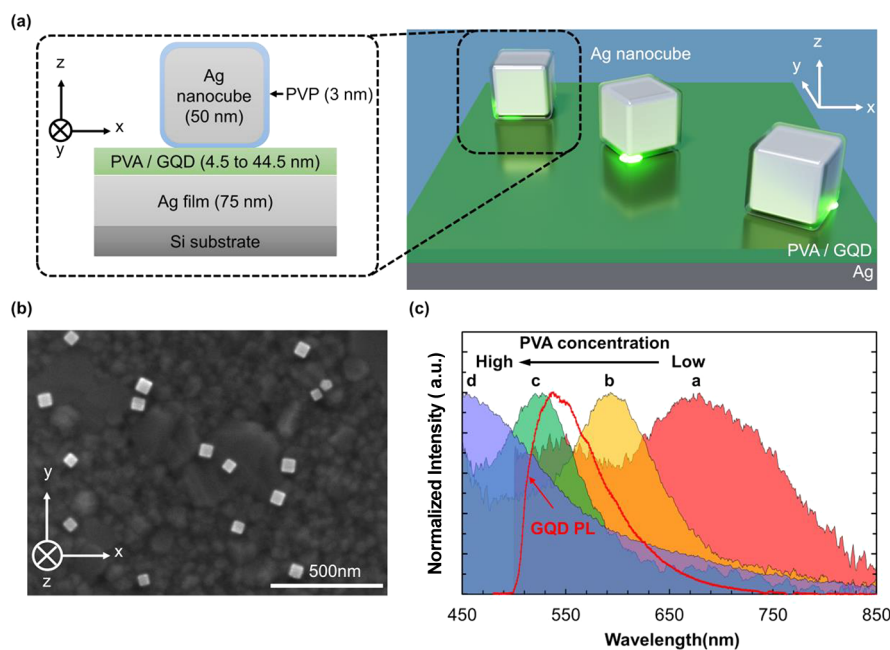


Figure 1. (a) Schematic of plasmonic nanogap cavities. They consist of 50 nm silver cubes surrounded by PVP, a PVA/GQD gap layer, and a silver film substrate on a Si wafer. On the right is shown a 3D illustration of the plasmonic nanogap cavities. In the gap spacer region, the electric field is strongly enhanced, leading to a fast emission lifetime and strong photoluminescence (PL) intensity. (b) SEM image with a top-down view (xy plane). (c) Normalized scattering spectra of the plasmonic nanogap cavities and normalized PL spectrum of GQDs in PVA (red line). All samples are made using the same conditions except for the concentration of the PVA, which is varied, and causing varying gap layer thicknesses during the spin coating process. a, 2.5 mg/mL PVA, 4.5 nm gap; b, 5.0 mg/mL PVA, 7.4 nm gap; c, 10 mg/mL PVA, 17.2 nm gap; d, 15 mg/mL PVA, 44.5 nm gap.

$$F = \frac{\gamma_{\text{sp}}}{\gamma_0} = \frac{3}{4\pi^2} \left(\frac{Q}{V_{\text{mode}}} \right) \left(\frac{\lambda}{n} \right)^3 \quad (2)$$

where Q is the cavity quality factor, V_{mode} is the mode volume, λ is the cavity's resonant wavelength, n is the refractive index of the medium, and γ_0 is the spontaneous emission rate of the emitter in free space. This formula indicates that a significant increase in the emission rate requires an optical resonator that can spatially confine light in a small mode volume for an extended period. Thus, a plasmonic nanocavity could exhibit a large Purcell factor due to the nanoscopic mode volume. In a properly designed cavity, the local density of states can be greatly increased, and GQDs in such a nanocavity are likely to experience a substantial acceleration of their spontaneous emission, as well as significant enhancement of their brightness. There are some reports of GQD fluorescence enhancement using single walled carbon nanotubes,¹⁴ silver nanoparticles,¹⁵ gold nanoslit cavities,¹⁶ silver nanoislands,¹⁷ magneto-plasmonic nanoparticles,¹⁸ silver nano-octahedrons,¹⁹ and gold nanoparticles.²⁰ However, the effect of shortening lifetime has not been discussed.

Here, we report lifetime enhancements of up to 288-fold and bright luminescence from GQDs by coupling them to the gap plasmon modes of nanopatch antennas. In this study, the plasmonic nanogap cavities are comprised of silver nanocubes separated from a silver film by a composite poly(vinyl alcohol) (PVA) and GQD spacer layer (PVA/GQD), as shown in Figure 1a. PVA has been previously reported as a good dispersion matrix of GQDs.²¹ We measured the mean size of the GQDs as 2.6 nm via dynamic light scattering (DLS) (see Supporting Information Figure S1). The size is smaller than the thickness of the typical gap layer which means that the

GQDs can be embedded in the nanopatch antennas. The thin films were prepared by spin coating of an aqueous solution of PVA and GQD on a 75 nm Ag film on a Si wafer. The concentration of GQDs was fixed at 1 $\mu\text{g}/\text{mL}$. The concentration of PVA was varied from 2.5 to 15 mg/mL in order to obtain different thicknesses of the PVA/GQD gap layer. Different gap spacer thicknesses were obtained depending on the PVA concentration and characterized by imaging ellipsometry (nanofilm ep4, Accurion Inc.) (Figure S1). Fabricating PVA/GQD layers with higher concentrations of PVA resulted in a lower refractive index, which is explained by the lower refractive index of PVA relative to that of GQDs. Furthermore, there was a correlation between PVA concentration and film thickness: a higher concentration of PVA resulted in a thicker PVA/GQD layer, ranging from 4.5 to 44.5 nm. The standard concentration utilized for samples was 10 mg/mL PVA solution, which resulted in an ~ 17.2 nm gap layer. Next, 50 nm colloidal silver nanocubes with a poly(vinylpyrrolidone) (PVP) coating were spin-coated onto the PVA/GQD gap layer. Dispersion of silver nanocubes on PVA/GQD was confirmed by SEM (Figure 1b). Very little aggregation of the nanocubes was observed. A more detailed fabrication procedure is described in the Sample Fabrication Section of the Supporting Information.

First, to evaluate the plasmon resonance, the scattering spectra of the plasmonic nanogap cavity samples were obtained and are shown in Figure 1c. The scattering peak wavelength red-shifted with increasing concentration of PVA and varied from 445 nm (2.5 mg/mL PVA, 4.5 nm gap sample) to 678 nm (15 mg/mL PVA, 44.5 nm gap sample). Previous work has shown that the plasmon resonance depends strongly on the nanocube size, gap layer thickness, fill fraction, shapes, and dielectric properties of the material in the gap.^{22–24} The

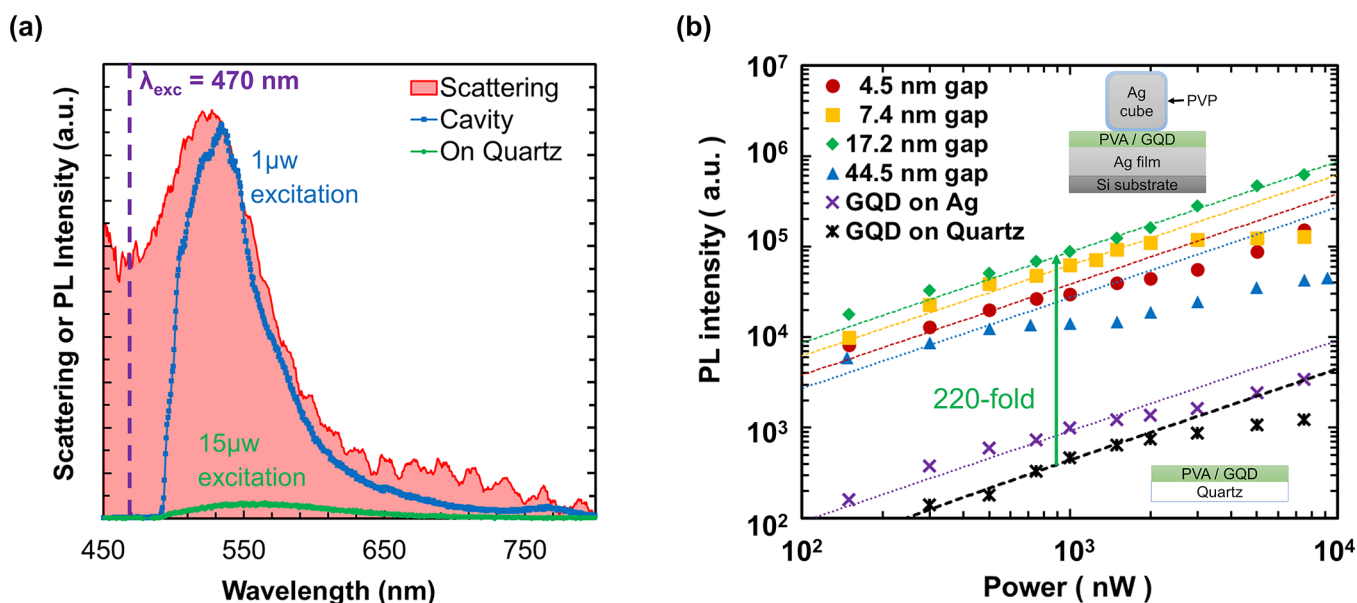


Figure 2. (a) PL intensity and scattering spectrum of a representative sample. The plasmon resonance is overlapped with both the excitation and emission wavelengths of the GQDs. (b) Excitation power dependence of the PL intensity for each plasmonic nanogap cavity sample and for two control samples, one consisting of PVA/GQD on quartz (black) and the other consisting of PVA/GQD on Ag without cubes (purple). The reference samples were made by a 10 mg/mL PVA solution recipe except for using a quartz substrate instead of an Ag-coated Si wafer or without Ag cubes. Dotted lines show linear fits to the data before saturation.

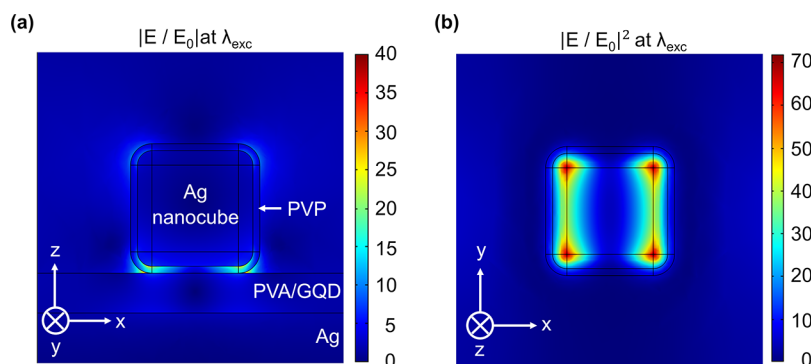


Figure 3. (a) Normalized simulated electric field enhancement at the excitation wavelength (λ_{exc}) shown in the xz plane. (b) Normalized electric field intensity ($|E/E_0|^2$) at the top of the PVA/GQD layer at $\lambda_{\text{exc}} = 470$ nm. A gap thickness of 17.2 nm consistent with that of films fabricated with 10 mg/mL PVA solution was used for this simulation. The observed symmetry breaking is due to the incident electric field being polarized in the transverse electric (TE) direction.

resonant wavelength of these samples was chosen to overlap with both the excitation wavelength ($\lambda_{\text{exc}} = 470$ nm) and the PL wavelength of the GQDs ($\lambda_{\text{em}} = 538$ nm). Next, PL measurements were performed using an imaging spectrometer (iHR 550, HORIBA, Ltd.) and a custom-built optical setup at room temperature (further details are provided in the Supporting Information). When plasmonic nanogap cavities were excited with a focused pulsed 80 MHz 470 nm laser (Ti-sapphire laser, second harmonic generation of 940 nm, Chameleon, Coherent Inc.), strong PL intensity at the wavelength overlapping with the scattering of the plasmonic nanogap cavities was observed (Figure 2a). When comparing samples with different concentrations of PVA, the highest fluorescence intensity was obtained from plasmonic nanogap cavities containing a 17.2 nm gap layer, primarily due to this sample having the best spectral overlap between the GQD emission and plasmon resonance, as seen in Figure 1c. For this sample, the emission intensity was 220 times larger than that of

a reference sample consisting of a PVA/GQD layer on a quartz substrate (Figure 2b).

The fluorescence enhancement factor (EF) of the nanopatch structure is quantified as¹²

$$\text{EF} = \frac{\gamma_{\text{ex}}}{\gamma_{\text{ex}}^0} \frac{\eta}{\eta^0} \frac{\text{QE}}{\text{QE}^0} \quad (3)$$

where γ_{exc} is the excitation rate at the excitation wavelength, η is the collection efficiency dependent on the numerical aperture (NA) of the first lens, QE is the photon quantum yield, and the superscript "0" indicates the quantities from the reference sample, in this case GQDs on a quartz substrate. The excitation rate enhancement, $\gamma_{\text{exc}}/\gamma_{\text{exc}}^0$ is proportional to $|E_{\text{exc}}/E_0^0|^2$,²⁵ where E_{exc} is the electric field at the excitation wavelength. In order to evaluate the electric field enhancement of the plasmonic nanogap cavities, finite-element method (FEM) simulations were performed using COMSOL. Using imaging ellipsometry and a Cauchy fit, the refractive index at

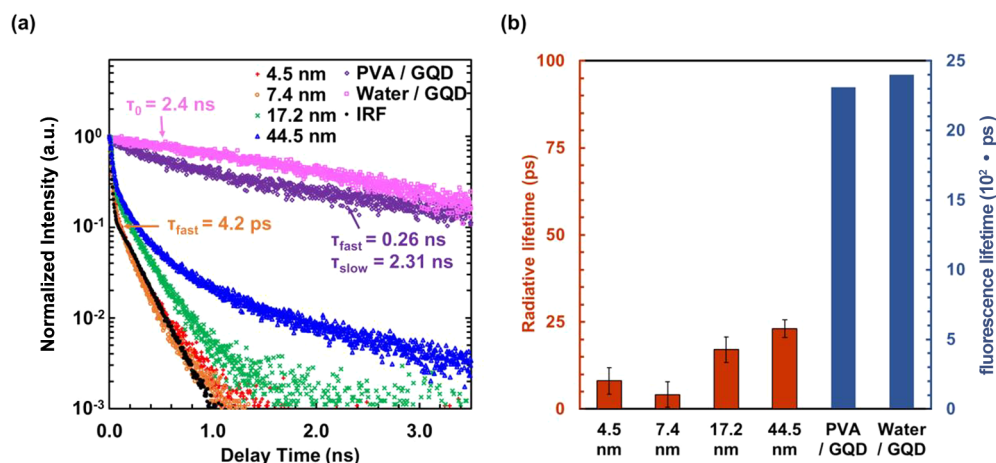


Figure 4. (a) Representative time-resolved PL curves from each sample studied. (b) τ_{fast} of plasmonic nanogap cavity samples (red bars, left axis), PVA/GQD and water solution (blue bars, right axis). The error bars are standard deviations as calculated from measurements on 20 different locations on each sample.

λ_{em} of the 10 mg/mL PVA sample was determined to be 2.16, the extinction coefficient 0.025, and the film thickness 17.2 nm (see Supporting Information Figure S1). Using these values, the calculated absorption spectrum agrees well with experimental results (Figure S3b). The fundamental resonance of this structure is shown in the electric field profile of Figure 3. The electric field enhancement occurred not only at the surface of the silver cubes with the PVP layer but also inside the PVA/GQD layer. The highest electric field enhancement, $|E_{exc}/E_{exc}^0|^2 = 71$, occurred at the top of the PVA/GQD layer adjacent to the silver. Further, eq 3 signifies that the PL intensity of coupled emitters is also proportional to the emission collection efficiency. The nanopatch structure has previously been shown to improve the collection efficiency with a 100X magnification, 0.9 NA objective lens by a factor of 4.5–5.5.^{12,13} Finally, eq 3 also signifies that the PL intensity depends upon the emission quantum yield, which is known to be enhanced by the nanopatch structure.^{12,13} The 220-fold enhancement of the fluorescence intensity is therefore attributed to a combination of the electric field enhancement at the excitation wavelength, the emission collection efficiency improvement, and the emission quantum yield enhancement.

To elucidate the PL enhancement contribution from uncoupled GQDs on the silver film, an additional reference sample was measured which consisted of GQD on an Ag film (without any nanocubes). The PL intensity of GQDs on the Ag film was 2.1-fold higher than GQDs on quartz (Figure 2). However, the enhancement factor was less than 1/100 compared with the largest enhancement factor obtained with the plasmonic nanogap cavities. This shows that the contribution from GQDs that are only coupled to the underlying Ag film is small. On the other hand, although the plasmon resonance of the 44.5 nm gap layer sample matched the excitation wavelength well, the PL intensity of the 44.5 nm gap layer sample (56-fold) was lower than that of the 17.2 nm gap layer sample (Figure 2b). To better understand this result, a FEM simulation of the electric field enhancement of the 44.5 nm gap layer sample was performed using the optical constants and the film thickness, as determined by imaging ellipsometry. The experimental absorption spectrum was observed to be broader than the simulation results (Figure S3c), likely resulting from inhomogeneities in the relatively thick PVA/GQD layer. The 44.5 nm gap layer sample had a higher

maximum electrical field enhancement than the 17.2 nm gap layer sample (Figure S4c). The highest $|E_{exc}/E_{exc}^0|^2$ was 115. However, the enhanced region was only in the vicinity of the silver cube and was not coupled with the silver substrate, resulting in weak field enhancement in most of the gap region. This lack of coupling to the silver film was due to the large thickness of the gap layer (44.5 nm). Therefore, GQDs in the gap were unlikely to be located in the enhanced hotspot, resulting in lower fluorescence enhancement. The field enhancement from a silver nanocube only extends ~20–30 nm,²⁶ which is less than the gap thickness of 44.5 nm for this sample. This further supports the hypothesis that substantial field enhancement in the gap only occurred within a close vicinity of the nanocubes.

Next, PL lifetime measurements were performed using time-correlated single photon counting (TCSPC). Details on the experimental method are provided in the Supporting Information. The intrinsic GQD lifetime of GQDs in water was measured to be $\tau_0 = 2.4$ ns, and the decay was well-modeled by a single exponential fit (Figure 4a), which is consistent with previous reports.¹⁰ The fluorescence decay of a PVA/GQD film on quartz was biexponential, where the fast and slow lifetimes were found to be $\tau_{fast} = 0.26$ ns (39%) and $\tau_{slow} = 2.31$ ns (61%). The radiative lifetimes of the plasmonic nanogap cavities were faster than the full width at half-maximum (fwhm) of the utilized avalanche photodiodes (APDa, Micro Photon Devices s.r.l., 35 ps fwhm). Hence, the lifetimes of the plasmonic nanogap cavities were calculated by deconvolution with the system's measured instrument response function (IRF) through a least-squares approach.²⁷ In general, deconvolution approaches can allow lifetimes substantially shorter than the fwhm of the IRF to be recovered. Twenty different locations on the sample were measured, and τ_{fast} was found to vary from 4.2 to 23 ps (Figure 4b). However, there is a limit imposed by the digitization of timing pulses with 4 ps time bins and therefore reliable recovery of lifetimes can only be performed down to an 8 ps lifetime, as given by the Shannon–Nyquist theorem.^{28,29} The fastest fluorescence lifetime of $\tau_{fast} \leq 8$ ps, which corresponded to a Purcell factor of over 288, was obtained from the 7.4 nm gap layer sample. The locational variability in τ_{fast} in a given sample was attributed to the positioning of individual emitters in the gap

Table 1. Overview of Enhanced Emission Lifetimes of Organic Dyes as Reported in the Literature

plasmonic structure	dye	fluorescence intensity enhancement	T_{fast}	ref.
Au bowtie dimers	quaterrylene	1340	<10 ps	35
Au nanosphere dimers	ATTO647N		60 ± 5 ps	36
Au nanospheres	carbon dots	20		37
Au nanorod and Au substrate	Nile blue	85	0.194 ns	38
Ag nanoparticle aggregation	cyanine	500	0.23 ns	39
Ag nanoparticle aggregation	A655	170	6.0 ± 0.8 ps	40
Ag nanoparticle aggregation	methylene blue	1000	6.7 ps	41
Ag nanoparticle aggregation	Cy5	12.3	0.94 ns	42
Ag nanocube and Au substrate	Ru dye	~ 110	0.7 ns	12
Ag nanocube and Ag substrate	GQD	~ 220	<8 ps	this work

relative to electric field enhancement “hot spots”, which increased the emitter LDOS.

The lifetime is related to the modified LDOS at the emitter position, where the LDOS is associated with the inner product of the electromagnetic field enhancement and the transition dipole moment of the emitter.⁴⁴ The electric field enhancement was simulated at both the emission wavelength of the GQDs ($\lambda = 538$ nm) and the center of the plasmon resonance ($\lambda = 590$ nm) by the same procedure as described above and shown in Supporting Figures S5 and S6, respectively. The maximum intensity of $|E/E^0|$ at the emission wavelength in the PVA/GQD gap region was observed for a gap thickness of 17.2 nm, and the maximum intensity of $|E/E^0|$ at the plasmon resonance wavelength was observed for a gap thickness of 7.4 nm, providing insights into the faster lifetimes for these samples. Furthermore, the orientation of the emitter transition dipoles relative to the electric field gap mode in the plasmonic nanogap cavities is an important factor in estimating the enhancement of the radiative lifetime.¹² The direction of the transition dipole moment of GQDs depends on the modifying chemical function groups at the edge.³⁰ The GQDs used here are water-soluble and contain an oxygen atom modification, and the modification position is random. Hence, the transition dipole moment of the GQDs is assumed to be random in the structures studied here. The GQDs have the maximum rate enhancement, $\gamma_{\text{sp}}/\gamma_0$, when the dipoles are vertically oriented; however, the experimentally observed enhancement is lower, as some emitters in the plasmonic nanogap cavities do not have optimally oriented transition dipoles.

This work used a nanopatch antenna structure, which has one of the highest LDOS of all nanophotonic architectures.³¹ According to eq 1, this, in turn, results in a high Purcell factor. Hence, the enhanced lifetimes reported in this work are consistent with previous literature reports of other emitters.¹² Compared with results of plasmonic enhancement of organic dyes, the τ_{fast} of ≤ 8 ps reported in this work is on the same order as other works (Table 1). However, the lifetimes we obtained were limited by the temporal resolution of the APDs utilized. Alternatively, upconversion techniques have been shown to measure lifetimes as short as 40 fs.³² This opens the possibility to characterize the lifetimes of plasmonically coupled GQDs at even higher speeds. The GQD nanopatch antenna structure has the potential to be the fastest system not only within plasmonically coupled GQDs but also within any plasmonically coupled organic dye.

In previous literature examples, organic dyes for which structural rotation allowed rapid excited state relaxation were found to have a lifetime of 2.2 ps.³³ Furthermore, aggregation in α -perylene crystals has been observed to result in

fluorescence lifetimes as short as 1.4 ps.³⁴ Both of these reported values are of the same order of magnitude as the results presented in this work. Thus, the nanoantenna structures utilized here provide fluorescence lifetime enhancement of organic dyes on par with more synthetically challenging relaxation techniques.

In conclusion, we demonstrated large enhancement of both the emission lifetime (288-fold) and the PL intensity (220-fold) of nanopatch-antenna-coupled GQDs. The fastest fluorescence lifetime is $\tau_{\text{fast}} \leq 8$ ps, which to the best of our knowledge is the highest speed reported in plasmon-coupled GQDs. The experimental results show good agreement with finite-element simulations, indicating the possibility of tailoring the fluorescence lifetime by suitably designing the plasmon resonance of the structure. The lifetime of ≤ 8 ps has the potential to provide control above 10 Gbps switching. Nanogap plasmonic cavities provide an alternative route to accelerate the lifetimes of organic dyes without special molecular design or crystallization processes. Furthermore, the PL wavelength of GQDs is tunable via the size of the GQDs or functionalization.⁴³ We demonstrated that the plasmon resonance wavelength was also changeable by only changing the thickness of the PVA/GQD gap layer via modifying the concentration of the PVA. The methods provided in this report will enable the design of plasmonic cavities with resonances matching the emission of any GQD variant of interest. The architecture presented here could be employed for high-speed displays and high-speed quantum communication in the visible band, since the GQD has been reported as an excellent single photon source.⁸

■ ASSOCIATED CONTENT

Supporting Information

The Supporting Information is available free of charge at <https://pubs.acs.org/doi/10.1021/acs.nanolett.1c03419>.

Materials, physical measurements, detailed sample fabrication procedure, detailed optical characterization, dynamic light scattering results, optical constants and thicknesses obtained by ellipsometry, FEM simulation results performed in COMSOL, and a histogram of fast decay components of each plasmonic nanogap cavity sample (PDF)

■ AUTHOR INFORMATION

Corresponding Author

Maiken H. Mikkelsen – Department of Electrical and Computer Engineering, Duke University, Durham, North Carolina 27708, United States; orcid.org/0000-0002-

0487-7585; Phone: +1 (919) 660-0185;
Email: m.mikkelsen@duke.edu

Author

Hiroyuki Kishida – Department of Electrical and Computer Engineering, Duke University, Durham, North Carolina 27708, United States

Complete contact information is available at:
<https://pubs.acs.org/10.1021/acs.nanolett.1c03419>

Notes

The authors declare no competing financial interest.

ACKNOWLEDGMENTS

M.H.M. acknowledges support from the Office of Naval Research (ONR) award no. N00014-17-1-2589 and the Army Research Office (ARO) award no. W911NF1610471. H.K. acknowledges support from the JSR Corporation, Japan.

REFERENCES

- (1) Yuan, F.; Wang, Y.-K.; Sharma, G.; Dong, Y.; Zheng, X.; Li, P.; Johnston, A.; Bappi, G.; Fan, J. Z.; Kung, H.; Chen, B.; Saidaminov, M. I.; Singh, K.; Voznyy, O.; Bakr, O. M.; Lu, Z.-H.; Sargent, E. H. Bright high-colour-purity deep-blue carbon dot light-emitting diodes via efficient edge amination. *Nat. Photonics* **2020**, *14*, 171–176.
- (2) Hasan, M. T.; Gonzalez-Rodriguez, R.; Ryan, C.; Coffey, J. L.; Naumov, A. V. Variation of Optical Properties of Nitrogen-doped Graphene Quantum Dots with Short/Mid/Long-wave Ultraviolet for the Development of the UV Photodetector. *ACS Appl. Mater. Interfaces* **2019**, *11*, 39035–39045.
- (3) Goswami, L.; Aggarwal, N.; Verma, R.; Bishnoi, S.; Husale, S.; Pandey, R.; Gupta, G. Graphene Quantum Dot-Sensitized ZnO-Nanorod/GaN-Nanotower Heterostructure-Based High-Performance UV Photodetectors. *ACS Appl. Mater. Interfaces* **2020**, *12*, 47038–47047.
- (4) Fadzilah, N. M. S.; Kadir, M. Z. A. A.; Shafie, S.; Rashid, S. A.; Wan Hasan, W. Z.; Norhanisah, J. TiO₂ Thickness and Graphene Quantum Dots Variation in Photoanode of Dye Sensitized Solar Cell Using Response Surface Methodology (RSM) Technique. *Solid State Science and Technology* [S.I.], v. 26, n. 2, p. 43–49, feb. 2019. ISSN 0127-9645. Available at: <https://myjms.mohe.gov.my/index.php/maspp/article/view/5255>. Date accessed: 30 dec. 2021.
- (5) Monroe, J. D.; Belevkov, E.; Er, A. O.; Smith, M. E. Anticancer Photodynamic Therapy Properties of Sulfur-Doped Graphene Quantum Dot and Methylene Blue Preparations in MCF-7 Breast Cancer Cell Culture. *Photochem. Photobiol.* **2019**, *95*, 1473–1481.
- (6) Nuengmatcha, P.; Sricharoen, P.; Limchoowong, N.; Mahachai, R.; Chanthai, S. The use of S₂O₈²⁻ and H₂O₂ as novel specific masking agents for highly selective “turn-on” fluorescent switching recognition of CN⁻ and I⁻ based on Hg²⁺-graphene quantum dots. *RSC Adv.* **2018**, *8*, 1407.
- (7) Zhao, S.; Lavie, J.; Rondin, L.; Orcin-Chaix, L.; Diederichs, C.; Roussignol, P.; Chassagneux, Y.; Voisin, C.; Mullen, K.; Narita, A.; Campidelli, S.; Lauret, J.-S. Single photon emission from graphene quantum dots at room temperature. *Nat. Commun.* **2018**, *9*, 3470.
- (8) Sreeprasad, T. S.; Rodriguez, A. A.; Colston, J.; Graham, A.; Shishkin, E.; Pallem, V.; Berry, V. Berry Electron-Tunneling Modulation in Percolating Network of Graphene Quantum Dots: Fabrication, Phenomenological Understanding, and Humidity/Pressure Sensing Applications. *Nano Lett.* **2013**, *13*, 1757–1763.
- (9) Zhuo, S.; Shao, M.; Lee, S.-T. Upconversion and Down-conversion Fluorescent Graphene Quantum Dots: Ultrasonic Preparation and Photocatalysis. *ACS Nano* **2012**, *6*, 1059–1064.
- (10) Roding, M.; Bradley, S. J.; Nyden, M.; Nann, T. Nann Fluorescence Lifetime Analysis of Graphene Quantum Dots. *J. Phys. Chem. C* **2014**, *118*, 30282–30290.
- (11) Berezin, M. Y.; Achilefu, S. Fluorescence Lifetime Measurements and Biological Imaging. *Chem. Rev.* **2010**, *110*, 2641–2684.
- (12) Akselrod, G. M.; Argyropoulos, C.; Hoang, T. B.; Ciraci, C.; Fang, C.; Huang, J.; Smith, D. R.; Mikkelsen, M. H. Probing the mechanisms of large Purcell enhancement in plasmonic nano-antennas. *Nat. Photonics* **2014**, *8*, 835–840.
- (13) Wu, Y.; Xu, J.; Poh, E. T.; Liang, L.; Liu, H.; Yang, J. K. W.; Qiu, C.-W.; Vallee, R. A. L.; Liu, X. Upconversion superburst with sub-2 μs lifetime. *Nat. Nanotechnol.* **2019**, *14*, 1110–1115.
- (14) Das, R.; Rajender, G.; Giri, P. K. Anomalous fluorescence enhancement and fluorescence quenching of graphene quantum dots by single walled carbon nanotubes. *Phys. Chem. Chem. Phys.* **2018**, *20*, 4527–4537.
- (15) Ran, C.; Wang, M.; Gao, W.; Yang, Z.; Shao, J.; Deng, J.; Song, X. A general route to enhance the fluorescence of graphene quantum dots by Ag nanoparticles. *RSC Adv.* **2014**, *4*, 21772–21776.
- (16) Bagra, B.; Zhang, W.; Zeng, Z.; Mabe, T.; Wei, J. Plasmon-Enhanced Fluorescence of Carbon Nanodots in Gold Nanoslit Cavities. *Langmuir* **2019**, *35*, 8903–8909.
- (17) Chae, W.-S.; Yun, J.; Nam, S.-H.; Lee, S.-G.; Yang, W.-G.; Yoon, H.; Park, M.; Jeon, S. Fluorescence Modulation of Graphene Quantum Dots Near Structured Silver Nanofilms. *ACS Appl. Mater. Interfaces* **2018**, *10*, 14079–14086.
- (18) Zou, F.; Zhou, H.; Tan, T. V.; Kim, J.; Koh, K.; Lee, J. Dual-Mode SERS-Fluorescence Immunoassay Using Graphene Quantum Dot Labeling on One-Dimensional Aligned Magnetoplasmonic Nanoparticles. *ACS Appl. Mater. Interfaces* **2015**, *7*, 12168–12175.
- (19) Wang, W.; He, D.; Duan, J.; Fu, M.; Zhang, X.; Wu, H.; Hu, Y.; Wang, Y. Modulated photoluminescence of graphene quantum dots in the vicinity of an individual silver nano-octahedron. *Phys. Chem. Chem. Phys.* **2014**, *16*, 4504–4509.
- (20) Sadrolhosseini, A. R.; Krishnan, G.; Safie, S.; Beygisangchin, M.; Rashid, S. A.; Harun, S. W. Enhancement of the fluorescence property of carbon quantum dots based on laser ablated gold nanoparticles to evaluate pyrene. *Optical Materials Express* **2020**, *10*, 2227–2241.
- (21) Kovalchuk, A.; Huang, K.; Xiang, C.; Marti, A. A.; Tour, J. M. Luminescent Polymer Composite Films Containing Coal-Derived Graphene Quantum Dots. *ACS Appl. Mater. Interfaces* **2015**, *7*, 26063–26068.
- (22) Lassiter, J. B.; McGuire, F.; Mock, J. J.; Ciraci, C.; Hill, R. T.; Wiley, B. J.; Chilkoti, A.; Smith, D. R. Plasmonic Waveguide Modes of Film-Coupled Metallic Nanocubes. *Nano Lett.* **2013**, *13*, 5866–5872.
- (23) Akselrod, G. M.; Huang, J.; Hoang, T. B.; Bowen, P. T.; Su, L.; Smith, D. R.; Mikkelsen, M. H. Large-Area Metasurface Perfect Absorbers from Visible to Near-Infrared. *Adv. Mater.* **2015**, *27*, 8028–8034.
- (24) Shen, Q.; Boyce, A. M.; Yang, G.; Mikkelsen, M. H. Polarization-Controlled Nanogap Cavity with Dual-Band and Spatially Overlapped Resonances. *ACS Photonics* **2019**, *6* (8), 1916–1921.
- (25) Yang, G.; Niu, Y.; Wei, H.; Bai, B.; Sun, H.-B. Sun Greatly amplified spontaneous emission of colloidal quantum dots mediated by a dielectric-plasmonic hybrid nanoantenna. *Nanophotonics* **2019**, *8*, 2313–2319.
- (26) Zhou, Y.; Chen, G.; Zou, S. Radiative Decay Rate Enhancement and Quenching for Multiple Emitters near a Metal Nanoparticle Surface. *J. Phys. Chem. C* **2021**, *125*, 2531–2536.
- (27) Enderlein, J.; Erdmann, R. Fast fitting of multi-exponential decay curves. *Opt. Commun.* **1997**, *134*, 371–378.
- (28) Becker, W. *Advanced Time-Correlated Single Photon Counting Techniques*; Springer: Berlin, 2005.
- (29) Wahl, M. *Time-Correlated Single Photon Counting*; PicoQuant GmbH: Berlin, 2017.
- (30) Javed, M. A.; Zhao, J.; Kilin, D.; Yu, T. Understanding of Light Absorption Properties of the N-Doped Graphene Oxide Quantum Dot with TD-DFT. *J. Phys. Chem. C* **2021**, *125*, 14979–14990.
- (31) Koenderink, A. F. Single-Photon Nanoantennas. *ACS Photonics* **2017**, *4*, 710–722.

(32) Akimoto, S.; Yokono, M.; Ohmae, M.; Yamazaki, I.; Tanaka, A.; Higuchi, M.; Tsuchiya, T.; Miyashita, H.; Mimuro, M. Ultrafast Excitation Relaxation Dynamics of Lutein in Solution and in the Light-Harvesting Complexes II Isolated from *Arabidopsis thaliana*. *J. Phys. Chem. B* **2005**, *109*, 12612–12619.

(33) Fujino, T.; Hirota, K.; Ohta, K.; Tahara, T. In-cell Viscosity Measurement Using a Fluorescence Up-conversion Microscope. *Chem. Lett.* **2008**, *37*, 1240–1241.

(34) Fujino, T.; Tahara, T. Femtosecond Fluorescence Up-conversion Microscopy: Exciton Dynamics in α -Perylene Microcrystal. *J. Phys. Chem. B* **2003**, *107*, 5120–5122.

(35) Kinkhabwala, A.; Yu, Z.; Fan, S.; Avlasevich, Y.; Mullen, K.; Moerner, W. E. Large single-molecule fluorescence enhancements produced by a bowtie nanoantenna. *Nat. Photonics* **2009**, *3*, 654–657.

(36) Busson, M. P.; Bidault, S. Selective Excitation of Single Molecules Coupled to the Bright Mode of a Plasmonic Cavity. *Nano Lett.* **2014**, *14*, 284–288.

(37) Kamura, Y.; Imura, K. Enhanced and Polarized Photoluminescence from Carbon Dot–Metal Nanoparticle Composites. *J. Phys. Chem. C* **2020**, *124*, 7370–7377.

(38) Wang, H.; Lin, Y.; Ma, P.; Zhong, Y.; Liu, H. Tunable fluorescence emission of molecules with controllable positions within the metallic nanogap between gold nanorods and a gold film. *J. Mater. Chem. C* **2019**, *7*, 13526–13535.

(39) Fu, Y.; Zhang, J.; Lakowicz, J. R. Largely Enhanced Single-Molecule Fluorescence in Plasmonic Nanogaps Formed by Hybrid Silver Nanostructures. *Langmuir* **2013**, *29*, 2731–2738.

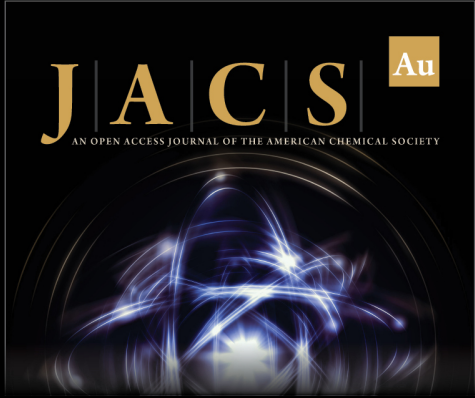
(40) Gill, R.; Tian, L.; Somerville, W. R. C.; Le Ru, E. C.; van Amerongen, H.; Subramaniam, V. Silver Nanoparticle Aggregates as Highly Efficient Plasmonic Antennas for Fluorescence Enhancement. *J. Phys. Chem. C* **2012**, *116*, 16687–16693.

(41) Gill, R.; Tian, L.; van Amerongen, H.; Subramaniam, V. Emission enhancement and lifetime modification of phosphorescence on silver nanoparticle aggregates. *Phys. Chem. Chem. Phys.* **2013**, *15*, 15734–15739.


(42) Liu, P.; Zhou, Y.; Guo, M.; Yang, S.; Felix, O.; Martel, D.; Qiu, Y.; Ma, Y.; Decher, G. Fluorescence-enhanced bio-detection platforms obtained through controlled “step-by-step” clustering of silver nanoparticles. *Nanoscale* **2018**, *10*, 848–855.


(43) Sk, M. A.; Ananthanarayanan, A.; Huang, L.; Lim, K. H.; Chen, P. Revealing the tunable photoluminescence properties of graphene quantum dots. *J. Mater. Chem. C* **2014**, *2*, 6954–6960.


(44) Ciraci, C.; Rose, A.; Argyropoulos, C.; Smith, D. R. Numerical studies of the modification of photodynamic processes by film-coupled plasmonic nanoparticles. *J. Opt. Soc. Am.* **2014**, *31*, 2601–2607.



JACS Au
AN OPEN ACCESS JOURNAL OF THE AMERICAN CHEMICAL SOCIETY

 Editor-in-Chief
Prof. Christopher W. Jones
Georgia Institute of Technology, USA

Open for Submissions 

pubs.acs.org/jacsau  ACS Publications
Most Trusted. Most Cited. Most Read.